

# Homology Modeling of Human Serum Carnosinase, a Potential Medicinal Target, and MD Simulations of Its Allosteric Activation by Citrate

Giulio Vistoli,<sup>\*,†</sup> Alessandro Pedretti,<sup>†</sup> Matteo Cattaneo,<sup>†</sup> Giancarlo Aldini,<sup>†</sup> and Bernard Testa<sup>‡</sup>

*Istituto di Chimica Farmaceutica, Facoltà di Farmacia, Università di Milano, Viale Abruzzi 42, I-20131 Milano, Italy, and Department of Pharmacy, University Hospital Centre (CHUV), Rue du Bugnon, CH-1011 Lausanne, Switzerland*

Received February 23, 2006

Recent biochemical and clinical evidence implicates human serum carnosinase in a variety of pathological conditions, such as neurological disorders and diabetic nephropathy, suggesting that this enzyme is of potential interest as a novel medicinal target. The present study was undertaken with a view to model the serum carnosinase and its catalytic site and to unravel the molecular mechanism by which citrate ions increase the catalytic efficiency of serum carnosinase. A homology model of the enzyme was obtained on the basis of  $\beta$ -alanine synthetase, and its active center was found to bind known substrates carnosine, homocarnosine, and anserine in a binding mode conducive to catalysis. Citrate ions were shown to bind at only three well-defined sites involving both ion pairs and hydrogen bonds. Molecular dynamics simulations evidenced that citrate binding had a remarkable conformational influence on the 3D structure of carnosinase, increasing the binding affinity (i.e., binding score) of carnosine to the catalytic site. This is one of the first reports documenting the molecular mechanism of an allosteric enzyme activator using MD simulations.

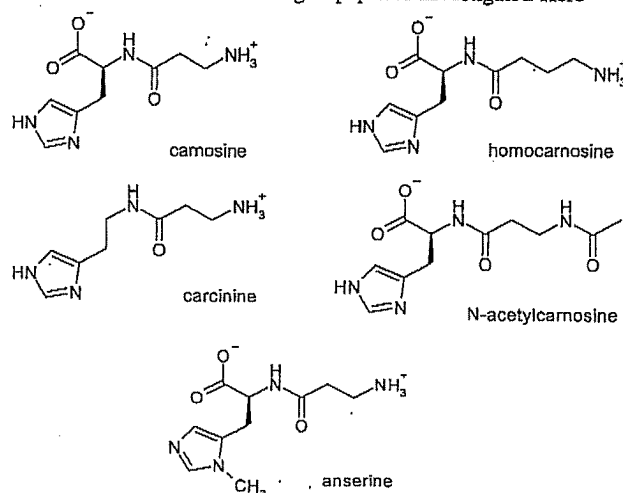
## Introduction

The dipeptide carnosine ( $\beta$ -alanine-L-histidine) represents the archetype of a series of histidine-containing dipeptides, such as homocarnosine, carcine, *N*-acetylcarnosine, and anserine (Chart 1).<sup>1,2,3</sup> The complete role of these dipeptides is still unknown, even though their function has been studied intensively in recent years. Available studies indicate that carnosine can act as a cytosolic buffer,<sup>4</sup> an antioxidant,<sup>5</sup> an  $\alpha,\beta$ -unsaturated carbonyl scavenger,<sup>6</sup> and an antiglycation agent.<sup>7</sup> Moreover, homocarnosine can represent a GABA reservoir, mediating the antiseizure effects of GABAergic therapies.<sup>8</sup>

Carnosine is synthesized by carnosine synthetase<sup>9</sup> (EC 6.3.2.11) in many tissues<sup>10</sup> and hydrolyzed by ubiquitous dipeptidases (also called carnosinases), which belong to metalloproteases.<sup>11</sup> Until now, two isoforms of carnosinase have been characterized. The first enzyme is a cytosolic form (also named tissue carnosinase, CN2, EC 3.4.13.18), which acts as a nonspecific dipeptidase with broad substrate specificity and being strongly inhibited by bestatin.<sup>12</sup> The second enzyme is known as serum carnosinase<sup>13</sup> (CN1, EC 3.4.13.20) and is characterized by its distribution in the plasma and brain, its ability to also hydrolyze anserine and homocarnosine, and its absence in nonprimate mammals except in the Syrian golden hamster.<sup>14</sup> Recently, the cDNA codes for the two carnosinases were identified and expressed, confirming many biophysical and biochemical properties of the two isoforms.<sup>15</sup>

Experimental evidence shows that serum carnosinase is present in solution as a homodimer, despite the fact that the monomer alone appears to be catalytically self-sufficient.<sup>13</sup> Although the nature of the metal ion in serum carnosinase remains unknown, it is likely that two  $\text{Zn}^{2+}$  ions are involved in the catalytic site because of its homology with the M20 family of metalloproteases.<sup>15</sup> Finally, serum carnosinase is activated by  $\text{Cd}^{2+}$  and citrate ions,<sup>13</sup> although it is unknown whether

Chart 1. Histidine-Containing Dipeptides Investigated Here



citrate promotes enzyme dimerization and/or improves the catalytic efficiency of the single monomer by acting as an allosteric activator.

There is a large body of evidence demonstrating that serum carnosinase is involved in some important pathological conditions. Thus, low levels of serum carnosinase is responsible for elevated concentrations of homocarnosine in the brain and cerebrospinal fluid (homocarnosinosis),<sup>16</sup> a deficiency accompanied by neurological disorders, such as paraplegia, retinitis pigmentosa, and progressive mental deficiency.<sup>17</sup> Decreased concentrations of serum carnosinase have been also observed in patients with Parkinson's disease, multiple sclerosis, or after a cerebrovascular accident.<sup>18</sup> It has also been suggested that the monitoring of serum carnosinase may be useful to predict the clinical outcome of patients with acute stroke.<sup>19</sup> Furthermore, a recent study<sup>20</sup> has demonstrated that diabetic patients with genetically based low serum carnosinase levels (*Mannheim variant*) are less susceptible to nephropathy, suggesting some beneficial effects of carnosine against the adverse effects of high glucose levels in renal cells.

\* To whom correspondence should be addressed. Tel: 39 3-503-175-45. Fax: 39 02-503-1 75-65. E-mail: giulio.vistoli@unimi.it.

<sup>†</sup> Università di Milano.

<sup>‡</sup> University Hospital Centre.

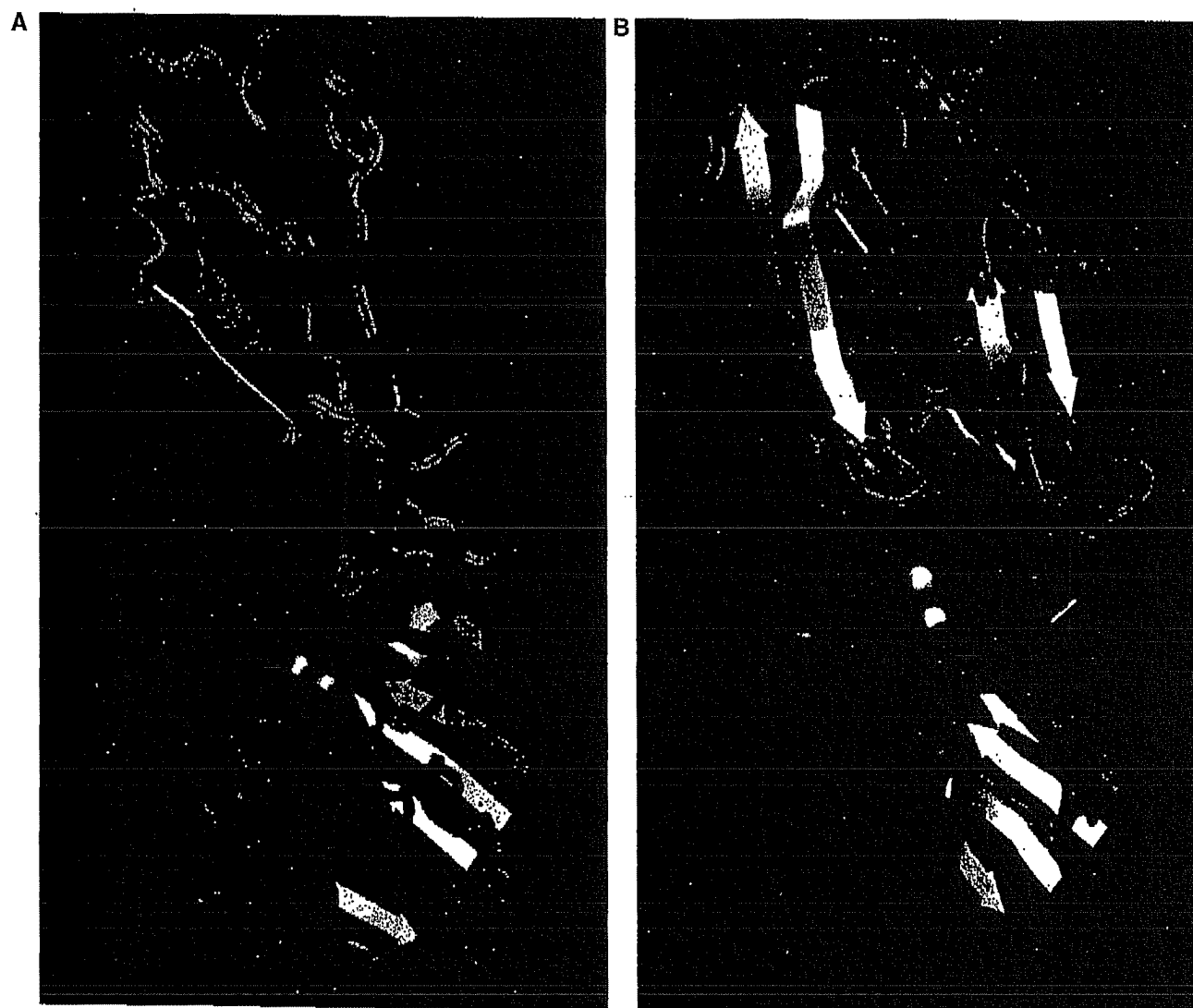


**Figure 1.** Three-dimensional ribbon of the two models of human serum carnosinase generated in this study. The lid domain is colored in green, whereas the catalytic domain is in blue. The metal ions are displayed in silver. (A) Three-dimensional model based on  $\beta$ -alanine synthetase. (B) Three-dimensional model based on PepV.

Taken globally, these studies shed light on the promising roles of serum carnosinase and suggest a therapeutic usefulness of either inhibiting (e.g., in diabetes) or activating (e.g., in homocarnosinosis) the enzyme. The design of serum carnosinase inhibitors can be based on our detailed knowledge of its catalytic site and its recognition capacities. In contrast, almost no information is currently available to design serum carnosinase activators, but a possible path to such information may be opened by exploring the molecular mechanism by which citrate activates the enzyme. Indeed, such an understanding may unveil novel approaches to increase the activity of serum carnosinase, for example, by permitting the rational design of citrate-like, non-toxic allosteric modulators.

To approach this objective, we first undertook to generate a 3D model of human serum carnosinase by homology modeling techniques. The resulting model was then validated by docking a few histidine-containing dipeptides, thus unravelling the pharmacophoric pattern of the catalytic site. In a third step, molecular dynamics (MD) simulations were used to examine, in molecular detail, the effects of citrate ions on the activity of serum carnosinase.

## Results

**Structural Features of Carnosinase.** As described in the Computational Methods section, two homology models of serum carnosinase were generated using PepV dipeptidase and  $\beta$ -alanine synthetase as templates. However, the first model was discarded because of the inaccessibility of its catalytic site, and all-docking analyses and MD simulations were carried out using the model derived from  $\beta$ -alanine synthetase.

Figure 1A depicts the serum carnosinase model obtained with  $\beta$ -alanine synthetase as the template, showing an ellipsoidal shape with axes equal to 80 and 40 Å. The 3D structure of the protein consists of two distinct domains, namely, the upper or lid domain and the lower (catalytic) domain. The latter consists of residues from Ser1 to Pro275 and from His390 to His481, whereas the lid domain comprises the residues from Leu276 to Leu389. Zinc ions are located in the catalytic domain and are involved in interactions with His106, Gly115, Asp139, Glu173, Glu174, and two water molecules, as seen in  $\beta$ -alanine synthetase. The water molecules were kept during the modeling of the protein but were deleted in docking calculations and MD simulations to facilitate substrate interactions. With-

Table 1. Docking Scores for the Investigated Dipeptides

di peptide	hydrolysis <sup>a</sup>	best score <sup>b</sup>	average of first 10 frames <sup>b</sup>	average of first 20 frames <sup>b</sup>	average of all 30 frames <sup>b</sup>
carnosine	HYD	-40.25	37.21	35.59	34.12
homocarnosine	HYD	-40.21	37.19	35.74	34.41
carcine	NON-hyd	-35.08	32.13	30.37	29.12
<i>N</i> -acetylcarnosine	NON-hyd	-34.10	29.26	27.35	25.66
anserine	HYD	-30.75	25.96	23.60	21.99

<sup>a</sup> Because of large discrepancies among experimental literature data, a simple dichotomic classification is used here. HYD = hydrolyzed dipeptides; NON-hyd = unhydrolyzed dipeptides. <sup>b</sup> Score values in kcal/mol.

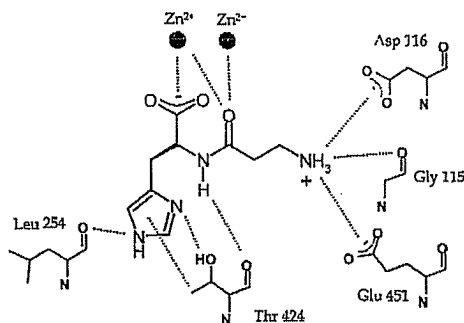


Figure 2. Two-dimensional representation of the interaction pattern between carnosinase and its substrate carnosine. The model shows how the enzyme recognizes (binds) the ammonium group, the carboxylate group, and the unsubstituted imidazole ring. The amido bond is simultaneously bound for recognition and polarized for catalysis.

out water molecules, the side chain of Asp116 bridges the two zinc ions.

The catalytic domain consists of a series of antiparallel  $\beta$ -sheets surrounded by a crown of  $\alpha$ -helices, whereas the lid domain shows some antiparallel  $\beta$ -sheets in the interface with the catalytic domain and two  $\alpha$ -helices in the upper surface. Lid and catalytic domains are connected by a random coil region that can act as a hinge permitting the relative movements of the domains during substrate recognition and enzyme activation. Moreover, the contacting surfaces of the two domains are noticeably rich in ionized residues; this generates a number of key ion pairs (e.g., Glu187 with Lys346 and Asp189 with Arg350) that stabilize the proper orientation of the domains.

Figure 1B shows that the second serum carnosinase model based on PepV dipeptidase<sup>21</sup> is comparable to the previous one but with the two domains clearly closer. In particular, this model shows a lid domain markedly larger than that in the  $\beta$ -alanine synthetase model consisting of antiparallel  $\beta$ -sheets in the interface with the catalytic domain and four  $\alpha$ -helices in the upper surface.

**Ligand Docking and Pharmacophoric Pattern.** Table 1 reports the scores of relevant histidine-containing dipeptides when docked with the serum carnosinase model based on  $\beta$ -alanine synthetase as the template. As seen in Table 1, carnosine shows the best score among these dipeptides. Interestingly, the same rank order is obtained considering the best solution, the average score of the first 10 complexes, the average score of the first 20 complexes, and the average score of all 30 complexes.

The best docking mode of carnosine was then used to define a recognition pharmacophore of serum carnosinase toward its substrates (Figure 2). The ammonium group of carnosine is seen to interact with the carboxylates of Asp116 and Glu451 and with the backbone carbonyl of Gly115. The carbonyl and carboxylate groups of carnosine also interact with the  $Zn^{2+}$  ions in the catalytic site. Polarization of the carbonyl group is thus

increased, an essential catalytic feature of hydrolases.<sup>22</sup> The backbone carbonyl of Leu254 forms a hydrogen bond with  $N^{\delta}$  in the imidazole ring. Like Thr424, it produces an interesting set of interactions, namely, a H bond with  $N^{\epsilon}$ , a second H bond with the amido group, and a hydrophobic interaction with the imidazole ring.

It is of relevance to point out that the interactions unraveled here involve both nitrogen atoms in the imidazole moiety, a fact that can explain the specificity of serum carnosinase toward histidine-containing dipeptides. Moreover, these interactions can explain the lower activity of serum carnosinase toward carnosine analogues with a substituted nitrogen in the imidazole ring, although the capacity of anserine to be hydrolyzed suggests that all imidazole-involving contacts are not required for enzyme recognition and catalysis.

Table 1 shows that homocarnosine has a high docking score identical with that of carnosine, and its interaction pattern is also very similar (data not shown). This result can be justified considering that the larger steric hindrance of homocarnosine can be compensated by its greater flexibility. As a result, homocarnosine can assume a bioactive conformation similar to that of carnosine in its best complex, and, thus, be a good substrate of the enzyme. This result is of significance because it confirms the capacity of serum carnosinase to hydrolyze homocarnosine and, thus, play an exploitable role in homocarnosinosis-induced disorders (see below).

Finally, the modest docking scores of carcine and *N*-acetylcarnosine can be rationalized considering that carcine lacks a carboxylate group, whereas *N*-acetylcarnosine lacks a charged ammonium group and is characterized by marked steric hindrance, which prevents its carbonyl group from interacting with the zinc ions.

Taken globally, the docking results afford an encouraging validation of our serum carnosinase model based on  $\beta$ -alanine synthetase, and they suggest a comprehensive and coherent interaction pattern between the enzyme and its ligands. Nevertheless, it must be remembered that docking calculations can simulate only the recognition phase between enzymes and their substrates, whereas the catalytic phase cannot be simulated by this approach. In other words, a given compound can be found to elicit good binding interactions and high score values with an enzyme, yet fail to possess an appropriate target group or fail to allow its binding in a catalytically productive mode, as seen with *N*-acetylcarnosine (results not shown).

It is worth emphasizing that the docking calculations were also used to select the best carnosinase model. Indeed, docking calculations were also performed for carnosine using the model based on PepV dipeptidase. The complexes obtained with the PepV dipeptidase model were of lower quality than those obtained with the  $\beta$ -alanine synthetase model, mainly because of the scarce accessibility of the catalytic site in the former model (results not shown).

**Docking of Citrate Ions.** Docking calculations of citrate ions to serum carnosinase led to some unexpected results (Figure 3). Indeed, the binding of the citrate ion was found to be restricted to three high-affinity sites on the protein surface (labeled  $\alpha$ ,  $\beta$ , and  $\gamma$  for clarity); all 30 complexes generated during the simulations exclusively involved these three sites. We found it highly surprising that the recognition of a small, flexible, and strongly negatively charged molecule such as the citrate ion by a protein surface rich in positively charged residues should occur exclusively on a few well-defined sites.

Figure 3 shows the best docking score for each binding site, revealing that the  $\alpha$  site is located in the region connecting the

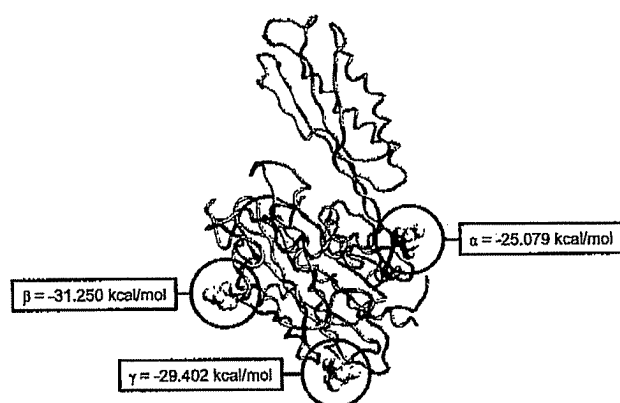


**Figure 3.** Solution clusters obtained with the 30 complexes between carnosinase and the citrate ion. The Figure shows the best solution for each binding site.

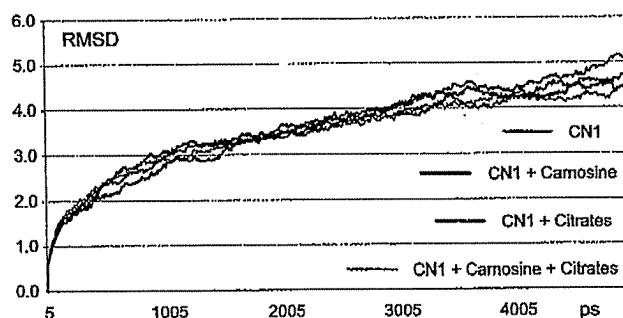


**Figure 4.** RMSD profiles for the four MD simulations performed with carnosinase (CN1), carnosinase with carnosine, carnosinase with three citrate ions, and carnosinase with carnosine plus three citrate ions.

two domains of serum carnosinase, whereas the  $\beta$  and  $\gamma$  sites are located in the lower region of the catalytic domain. In all cases, stabilization of the complexes was through ion pairs with positively charged residues (e.g., Lys405 and Arg409 in the  $\alpha$  site, Lys28 and Arg50 in the  $\beta$  site, and Arg65 in the  $\gamma$ ) and reinforced by H bonds (e.g., Tyr401 in the  $\alpha$  site, Gly25 and Tyr123 in the  $\beta$  site, and Gly63 and Ser94 in the  $\gamma$  site). Indeed, the citrate ion never elicited three ionic bonds in the binding sites because at least one carboxylate was involved only in H bonding. This suggests that ionic bonds, despite their importance, are not sufficient to stabilize citrate–carnosinase complexes and that H bonds, van der Waals interactions, and mutual adaptability also play a key role. This model may also explain the high specificity of the citrate recognition sites in carnosinase.

#### Fluctuations in the Free versus Complexed Carnosinase.

Four MD simulations were performed involving carnosinase alone, carnosinase with three citrates, carnosinase with carnosine, and carnosinase with citrates plus carnosine. First, the root-mean-square deviation (RMSD) profiles of carnosinase backbone atoms was analyzed relative to the initial structure (i.e., after the heating phase). This was undertaken to assess fluctuations during simulations. Figure 4 shows that the four MD simulations yielded similar RMSD profiles, thus confirming the overall stability of all systems. Although 5 ns may not be sufficient to entirely explore the conformational space of the structure of unliganded serum carnosinase, its conformational rearrangements described below clearly appear to be mainly due to the dynamic response of the enzyme and not to random structural distortions. In particular, the sole RMSD profile, which is somewhat different, is that seen with carnosinase in the sole presence of three citrates, which shows slightly higher RMSD

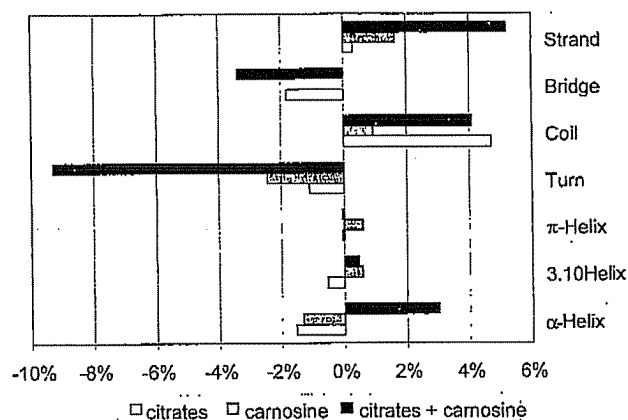


**Figure 5.** Percent change of each type of secondary structure in the three trajectories, compared to the trajectory of carnosinase without the ligand (zero values). White bars: carnosinase with citrates. Grey bars: carnosinase with carnosine. Black bars: carnosinase with citrates plus carnosine.

values postulated to be due to an unfolding effect caused by the citrate ions.

This effect of citrate ions was confirmed by separately calculating the percentage of each type of secondary motif. The last 4 ns of each trajectory was monitored by sampling 40 frames (1 frame/100 ps) and calculating the percentage of each type of secondary motif for each frame. The changes were expressed as differences between the free (taken as the zero value) and complexed carnosinase (namely, carnosinase with citrates, carnosinase with carnosine, and carnosinase with carnosine plus citrates).

As shown in Figure 5, the simultaneous binding of carnosine plus three citrates (black columns) caused an effect that was not the mere sum of the separate effects of citrates (empty columns) and carnosine (grey columns). Indeed, the citrates bound in the absence of carnosine induced a partial unfolding of the protein with an increase in coil structures, whereas the carnosinase–carnosine complex showed a modest decrease in the  $\alpha$ -helix and turn motifs, a decrease compensated by an increase in strand and coil structures.

In contrast, carnosine and citrates together (black columns in Figure 5) induced an increase in the percentage of  $\alpha$ -helix and strand motifs, with a corresponding decrease in the percentage of bridge and turn motifs. In particular, the increase in  $\alpha$ -helix abundance distinguishes this complex from the others, suggesting that the simultaneous binding of carnosine and citrates induces a net shift from turn to  $\alpha$ -helix motifs.

To reveal which protein segments were affected most by the presence of citrates, carnosine, or both, the relative time spent by each residue in a given secondary motif was also calculated over the 40 sampled frames. This was done for free carnosinase and its three complexes. The results are expressed as the percent change relative to free carnosinase (taken as the zero value). Figure 6A and B show that the simultaneous presence of carnosine plus citrates induced a clear tendency from turn to  $\alpha$ -helix rearrangements in the His390–Ala404 segment (Figure 6A and B), which is a connecting region between the lid domain and the catalytic domain (Figure 6C).

Moreover, Figure 7A shows that carnosine and citrate together induced a marked stabilization of the  $\alpha$ -helix structure of the His354–Ser373 segment, which is located in the upper surface of the lid domain (Figure 7B). The stabilization of the lid domain and the changes in the region connecting the two domains are postulated to be implicated in a conformational

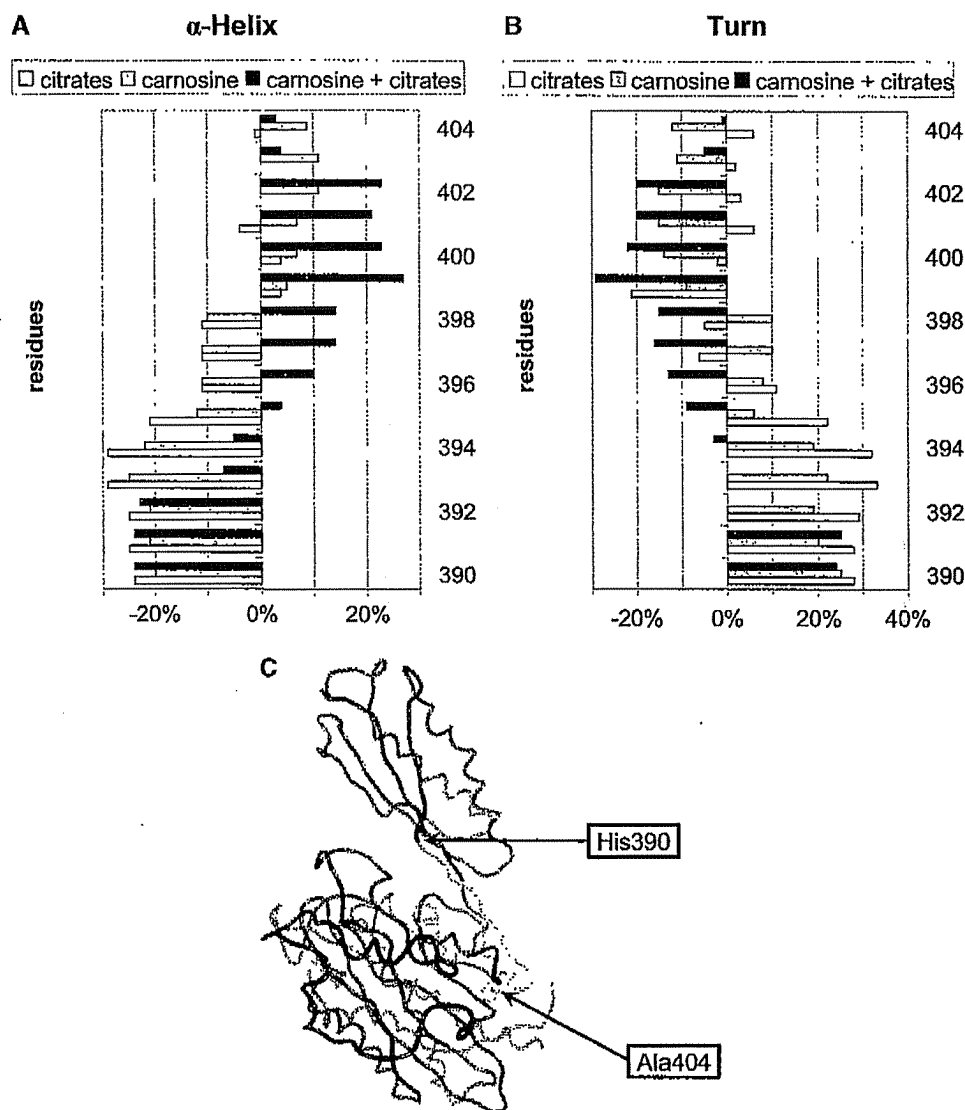


**Figure 6.** Conformational changes observed during the MD simulations in the His390–Ala404 segment during the three trajectories. The results are expressed as the percent of change relative to free carnosinase (taken as the zero value). White bars: carnosinase with citrates. Grey bars: carnosinase with carnosine. Black bars: carnosinase with citrates plus carnosine. (A) Percent changes in relative time spent in an  $\alpha$ -helix environment by each residue in the His390–Ala404 segment. (B) Percent changes in relative time spent in a  $\beta$ -turn environment by each residue in the His390–Ala404 segment. (C) Position of the His390–Ala404 segment in the connecting region between the two domains of carnosinase.

shift, which can modulate the accessibility of the catalytic site (see below).

The changes in secondary structure around all carnosinase residues were carefully checked, but the results were not as clear as those described in Figures 6 and 7, and their analysis did not reveal any other significant conformational transition. In other words, the conformational changes in the considered segments demonstrate that a small molecule such as the citrate ion can induce significant and specific structural effects in protein regions far away from its binding sites.

**Evidence for an Allosteric Effect of Citrate Ions.** Interestingly, the most evident conformational shifts observed in the carnosinase–carnosine–citrate complex concern the lid domain, whereas no marked conformational changes were seen in the catalytic domain. To shed light on the possible effects of citrate on the catalytic domain, the docking scores for the carnosinase–carnosine complexes with and without citrates were evaluated by sampling one frame each for 0.1 ns for the first ns, one frame each for 0.4 ns for the remaining 4 ns, and submitting them to FlexX to obtain the corresponding scores.

Figure 8 shows the score profiles as calculated during the two simulations, revealing that the presence of the three citrates in their respective binding sites leads to better scores for the binding of carnosine. Indeed, in both cases, a worsening of docking scores was observed during the first ns (the equilibration phase) mainly due to an initial rearrangement of the catalytic site. But in the presence of citrates, this worsening was overcome by a progressive improvement of score values that reached their minimum after about 3 ns and then remained lower by about 20 kcal/mol than the scores without citrates. Noticeably, in both simulations, the best score was reached after 3 ns, but the difference between the two lowest scores (–29.99 kcal/mol without citrates vs –54.77 kcal/mol in the presence of citrates) affords impressive evidence for an effect of citrates on the affinity of carnosinase for carnosine.

When analyzing the various complexes and their stabilizing interactions, we found that the presence of citrate ions induced a significant increase in hydrophobic/van der Waals contacts. This may mean that citrate ions are able to influence the catalytic site by improving the mutual adaptability between the enzyme

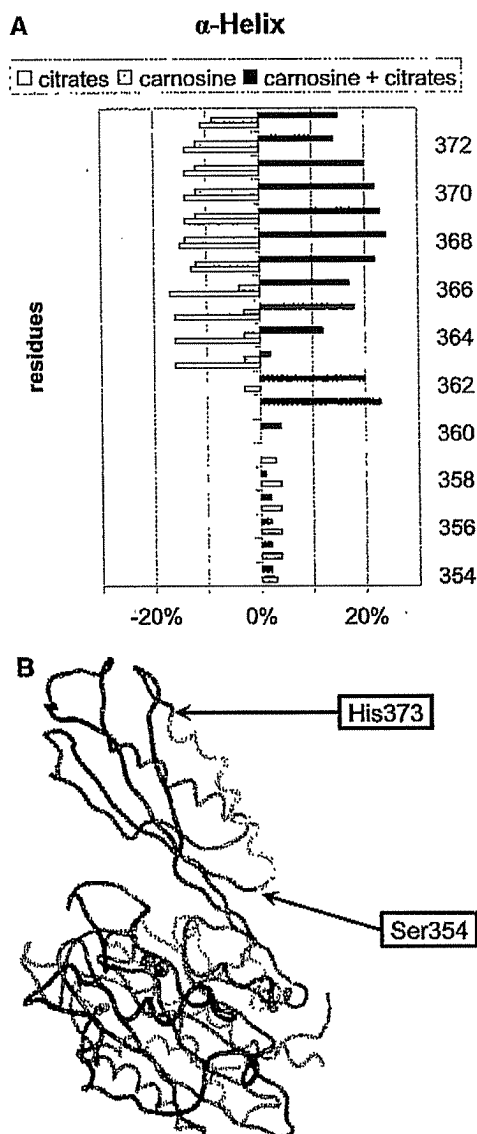


**Figure 7.** Conformational changes observed during the MD simulations in the His354–Ser373 segment during the three trajectories. The results are expressed as the percent of change relative to free carnosinase (taken as the zero value). White bars: carnosinase with citrates. Grey bars: carnosinase with carnosine. Black bars: carnosinase with citrates plus carnosine. (A) Percent changes in relative time spent in an  $\alpha$ -helix environment by each residue in the His354–Ala373 segment. (B) Position of the His354–Ser373 segment in the upper surface of the lid domain.

and substrates. Clearly, the key polar interactions that activate carnosinase (e.g., the interaction between zinc ions and the carbonyl group in the substrate) are independent of the presence of citrate, but the increased carnosinase affinity induced by citrates can be explained by the emergence of several additional hydrophobic/Van de Waals interactions.

To validate the results with citrates, we performed 1 ns MD simulations of the carnosinase–carnosine complex in the presence of (1) only one citrate molecule (one simulation for each citrate position) and (2) 9 chlorine ions in place of the  $3 \times 3$  carboxylate groups in the citrates. The results indicated very modest effects on the folding of serum carnosinase (data not shown), suggesting that (1) the effects of citrates cannot be explained by mere electrostatic shielding effects and that (2) all three citrates are simultaneously required to obtain the described allosteric effect. This last finding is of interest because

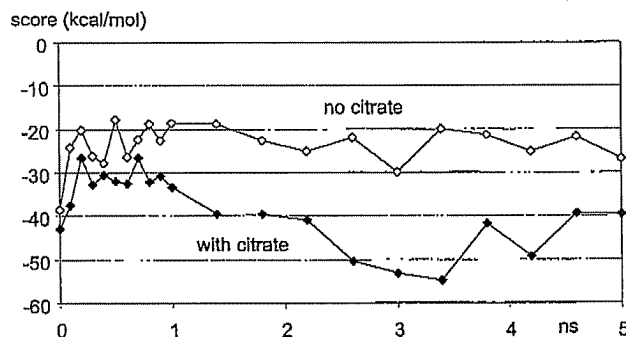


**Figure 8.** Effects of the presence of three citrates on the docking score of the carnosinase–carnosine complex during the molecular dynamics simulation. The graph reports the docking scores calculated from the frames stored every 0.1 ns during the first ns and every 0.4 ns during the remaining 4 ns.

it suggests a synergetic cooperation between three citrate ligands and invites experimental verification.

### Conclusions and Outlook

In our opinion, the most unexpected information to emerge from this study is the molecular mechanism by which citrate ions act as allosteric activators of human serum carnosinase. Allosteric transitions were discovered in the early 1960s by Monod and his eminent colleagues.<sup>23,24</sup> Since then, innumerable articles have been published showing the phenomenon to exist in enzymes, receptors, transporters, and ion sensors.<sup>25–31</sup> Tools applied to assess allosteric transitions include X-ray crystallography, enzyme kinetics and functional responses, protein engineering, and site-directed mutagenesis. To the best of our knowledge, little if anything has been done in silico using molecular modeling and molecular dynamics approaches. This article could therefore be one of the first reports detailing the molecular mechanism of an allosteric enzyme activator using molecular dynamics simulations.

Inhibition of serum carnosinase may be a useful therapeutic approach in the treatment of diabetic nephropathy. Recently, it was found that a trinucleotide repeat in exon 2 of the serum carnosinase gene *CNDP1* was associated with nephropathy, whereas the shortest allelic form (*CNDP1 Mannheim*) associated with lower serum carnosinase levels was more common in the absence of nephropathy.<sup>20</sup> In other words, the number of leucine repeats in the leader peptide of the *CNDP1* serum carnosinase gene appears to be associated with susceptibility for diabetic nephropathy. These results also suggest that the design of serum carnosinase inhibitors could afford renal protection in diabetes, especially in the most exposed patients having an increased expression of carnosinase due to the trinucleotide repeat in the *CNDP1* exon 2. Our homology model of human serum carnosinase and especially of its catalytic site appears specific and explicit enough to allow the design of competitive inhibitors.

Furthermore, carnosine has been found as a bioactive peptide in several pathological conditions, but its rapid hydrolysis in blood limits its pharmacological application as a detoxifying agent toward cytotoxic metabolites involved in the pathogenic mechanisms of atherosclerosis, ischemia, and nephropathy. It would therefore be of potential interest to design carnosine mimetics that retain the favorable effects of carnosine but are resistant to carnosinase. Again, our homology model offers a first tool toward this objective.

There is thus a large body of evidence indicating that serum carnosinase can be considered a promising and novel drug target and that therapeutic effects can be achieved either by inhibiting

or activating the enzyme depending on the pathological state. Activation of serum carnosinase might prove an approach to treat carnosinemia/homocarnosinemia, a very rare (prevalence 1:500,000) inherited and incurable metabolic disorder characterized by severely impaired neurological functions and developmental delays, caused by serum carnosinase deficiency and leading to high serum and urine levels of homocarnosine/carnosine. Dietary restriction of carnosine was found to reduce homocarnosine and carnosine to normal levels but was ineffective or only slightly effective in improving the general state of patients, suggesting that neurological disorders are not associated with high serum levels of histidine-containing dipeptides but may be caused by an impaired metabolism of dietary carnosine that probably affects the content of histidine-containing dipeptides in tissues. Hence, a promising therapeutic approach might be to partially restore the activity of serum carnosinase by an as yet undefined mechanism. The results presented here bring consistent evidence for an allosteric activation of serum carnosinase, identify three allosteric sites in the protein, and suggest a molecular mechanism by which the enzyme's activity is increased.

But whether inhibitors or allosteric activators, the design of compounds acting on carnosinase would be of significant value to gain a better understanding of the physiopathological roles of the enzyme and the substrates whose concentration it regulates. Indeed, the biological function of these substrates remains poorly known, and findings of clinical importance may be down the road. For example, a significant decrease in serum carnosinase activity has been found in patients undergoing heart surgery, suggesting that this might be a functional mechanism to protect against ischemic brain damage.<sup>32</sup>

### Computational Methods

**Construction of Carnosinase.** The amino acid sequence of human serum carnosinase (CN1) was retrieved from the Genebank/EBI Data Bank (accession number: AX139747<sup>33</sup>). The primary transcription sequence was submitted to the Signal IP 3.0 Server<sup>34,35</sup> to predict the cleavage site of the signal peptide. Predictions show the highest probability of cleavage between Ser27 and Ser28.

The primary sequence was submitted to Fugue,<sup>36</sup> an on-line sequence-structure homology recognition software that generates realistic models recognizing distant homologies by sequence-structure comparison. The best model produced by Fugue was based on the structure of PepV dipeptidase from *Lactobacillus delbrueckii*<sup>37</sup> (pdb id: 1LFW) as the template. Because this protein has been cocrystallized with an inhibitor (namely, AEP, 3-[(1-amino-2-carboxy-ethyl)-hydroxy-phosphinoyl]-2-methyl-propionic acid), the catalytic site was poorly accessible and could not accommodate any ligand without distorting its conformation. Hence, this model was discarded, and a more suitable model was searched for among the 20 solutions proposed by Fugue.

Results from the second to seventh rank were ignored because they predict less than 40% of the carnosinase sequence, and thus, the choice was for the eighth model based on the experimental structure of  $\beta$ -alanine synthetase from *Saccharomyces kluyveri*<sup>38</sup> (pdb id: 1R3N) as the template. This choice was justified by three main reasons: (1) this model predicts the highest percentage of carnosinase sequence leaving a few short unpredicted fragments; (2) the homology percentage between human serum carnosinase and  $\beta$ -alanine synthetase (as computed by using pairwise alignment) is significant (52.6%) and comparable to that with PepV dipeptidase (58.3%); and (3) carnosine contains  $\beta$ -alanine in its structure, and thus, some structural analogies between the catalytic site of the enzymes (namely, carnosinase and  $\beta$ -alanine synthetase) are probable. What is more, the model based on  $\beta$ -alanine synthetase shows a more accessible catalytic site, and indeed, docking analyses and MD simulations described here are performed with this model.

Specifically, the missing fragments in the selected carnosinase model were Ser1-Ala7, Ala67-Asp78, Arg114-Gly115, Arg190-Ile200, Val371-Asn379, and Phe431-Ile434. The four longest fragments (i.e., Ser1-Ala7, Ala67-Asp78, Arg190-Ile200, and Val371-Asn379) were separately resubmitted to Fugue, selecting the model best fitting the remaining backbone, whereas the two shortest fragments (i.e., Arg114-Gly115 and Phe431-Ile434) were manually added using the VEGA software.<sup>39</sup>

With the full-length backbone constructed, side chains and hydrogen atoms were added using VEGA. To remain compatible with physiological pH values, the side chains of Arg, Lys, Glu, and Asp were ionized, whereas His residues were considered neutral by default. The complete model was carefully checked to avoid unphysical occurrences, such as cis peptide bonds, wrong configurations, or colliding side chains. In these first phases and in the following steps, the model soundness was assessed using Procheck<sup>40</sup> and Verify3D.<sup>41</sup> A preliminary energy minimization was performed on the complete model to avoid high-energy interactions. During this minimization, the backbone atoms with the exception of atoms in the added fragments were kept fixed to preserve global folding.

To correctly arrange the zinc ions in the catalytic site of the model, metal ions and ligating residues were extracted from the structure of  $\beta$ -alanine synthetase and inserted in the carnosinase model by superimposing the C $\alpha$  carbon atoms of the coordinating residues to the corresponding atoms of carnosinase. All of these atoms except for the zinc ions were then deleted. Finally, an energy minimization was performed by fixing the atoms outside a sphere of 12 Å radius, centered on the middle point of the segment connecting the metal ions.

To gain a better relaxation and a more correct arrangement of the complete serum carnosinase model, a molecular dynamic simulation was performed in vacuo. The simulation was divided into a heating phase from 0 to 300 K (3 ps, i.e., 1 K/10 iterations) and an equilibration phase (0.5 ns) with constant temperature (300  $\pm$  25 K). During the simulation, only the zinc ions were kept fixed. The last frame of this simulation was further minimized and represented the starting point for the calculations to follow. This optimization procedure yielded a refined structure, which differs from the starting one for a RMSD equal to 1.67 Å (as computed from only the backbone atoms), suggesting an overall stability of the predicted folding of carnosinase.

**Building of Ligands.** A set of five histidine-containing dipeptides was considered (Chart 1), namely, carnosine ( $\beta$ -alanyl-L-histidine), homocarnosine ( $\gamma$ -aminobutyryl-L-histidine), carcine ( $\beta$ -alanyl-histamine), *N*-acetylcarnosine, and anserine ( $\beta$ -alanyl-3-methyl-L-histidine). All molecules were built using the VEGA software.<sup>39</sup> Carboxylic and amino groups were ionized, whereas the histidine imidazole ring was neutral (N<sup>+</sup>-H tautomer). After a preliminary minimization, partial charge attribution and geometry optimization were performed by the MOPAC 6.0 program (keywords = AM1, PRECISE, GEO-OK, MMOK).<sup>42</sup> The ligands underwent a Monte Carlo conformational search using the Quanta/CHARMm package (MSI, Burlington, MA), which generated 1000 conformers by randomly rotating the rotors. All conformers were minimized to avoid high-energy interactions, and the lowest energy one was used in docking calculations. The citrate ion was built in its tricarboxylate form using the same procedure.

**Docking of Ligands.** The software FlexX was used to perform docking analyses.<sup>43</sup> FlexX is a fast-automated docking program that takes ligand conformational flexibility into account by an incremental fragment technique. Docking analyses involved residues enclosed in a 12 Å radius sphere centered on the metal ions, generating 30 complexes for each ligand. Even if the exact mechanism of hydrolysis can only be postulated,<sup>22</sup> the docking parameters can be justified considering that at least one metal ion must be involved in catalysis, and thus, it is highly probable that substrates bind close to the zinc ions.

**Docking of Citrate.** To investigate the role of citrate as an allosteric activator, the tricarboxylate form of citric acid was docked into the carnosinase model. The docking was performed using FlexX<sup>43</sup> and involved the entire protein structure, but the metal ions

were removed to avoid an overestimation of electrostatic interactions that would have concentrated the best docking solutions close to the ions. As with substrate docking, 30 poses were generated.

**Molecular Dynamics.** Molecular dynamics simulations were performed with the following models: (1) carnosinase alone; (2) carnosinase with three citrate ions; (3) carnosinase with carnosine; and (4) carnosinase with carnosine and three citrate ions. All models were surrounded by a 10 Å layer of TIP3S water molecules as generated by the software VEGA.<sup>39</sup> Cylindrical boundary conditions (radius 45 Å; height 124 Å) were applied to the simulation space. The hydrated complexes underwent a preliminary minimization of the relative position of the solvent molecules to eliminate any high-energy interactions.

Molecular dynamic simulations were organized into an initial period of heating from 0 to 300 K over 3000 iterations (3 ps, i.e., 1 K/10 iterations) and a 5 ns simulation phase with constant temperature. Only frames memorized during the simulation phase were analyzed. To differentiate the allosteric effect of citrate from a mere charge-shielding effect, a MD simulation of the carnosinase-carnosine complex was carried out with 9 chloride ions instead of the 3 × 3 citrate carboxylates. The simulation lasted 1 ns with the same computational details. To better explain the effects of citrates, three MD simulations of the carnosinase-carnosine complex with a single citrate (one MD for each citrate binding site being occupied) were performed. The simulations lasted 1 ns with the same computational details.

**Computational Details.** The software NAMD<sup>44</sup> was used to perform energy minimizations and molecular dynamics, using Gasteiger's atomic charges and the atom types in the CHARMM v22 force field. The metal ions were kept fixed in all simulations. The MD simulations were analyzed using STRIDE<sup>45</sup> to determine the relative proportion of secondary structure motifs in the various frames.

All simulations had the following characteristics: minimizations with the conjugate gradients algorithm, convergence limit (RMS) = 0.01, maximal number of iterations = 5000; molecular dynamics with constant temperature in the range 300 ± 25 K by means of a thermostatic bath according to the Langevin's algorithm; and integration of Newton's equation each fs according to Verlet's algorithm. The frame stored 5000 iterations (5.0 ps) each, yielding 1000 frames per trajectory.

**Acknowledgment.** This work was supported by MURST grants (Cofinanziamento Programma Nazionale 2004).

## References

- Guiotto, A.; Calderan, A.; Ruzza, P.; Borin, G. Carnosine and carnosine-related antioxidants: a review. *Curr. Med. Chem.* **2005**, *12*, 2293–2315.
- Bauer, K. Carnosine and homocarnosine, the forgotten, enigmatic peptides of the brain. *Neurochem. Res.* **2005**, *30*, 1339–1345.
- Aldini, G.; Facino, R. M.; Beretta, G.; Carini, M. Carnosine and related dipeptides as quenchers of reactive carbonyl species: from structural studies to therapeutic perspectives. *Biofactors* **2005**, *24*, 77–87.
- Vaughan-Jones, R. D.; Spitzer, K. W.; Swietach, P. Spatial aspects of intracellular pH regulation in heart muscle. *Prog. Biophys. Mol. Biol.* **2006**, *90*, 207–224.
- Decker, E. A.; Livisay, S. A.; Zhou, S. A reevaluation of the antioxidant activity of purified carnosine. *Biochemistry (Moscow, Russ. Ed.)* **2000**, *65*, 766–770.
- Aldini, G.; Carini, M.; Beretta, G.; Bradamante, S.; Facino, R. M. Carnosine is a quencher of 4-hydroxy-nonenal: through what mechanism of reaction? *Biochem. Biophys. Res. Commun.* **2002**, *298*, 699–706.
- Seidler, N. W. Carnosine prevents the glycation-induced changes in electrophoretic mobility of aspartate aminotransferase. *J. Biochem. Mol. Toxicol.* **2000**, *14*, 215–20.
- Petroff, O. A.; Hyder, F.; Rothman, D. L.; Mattson, R. H. Homocarnosine and seizure control in juvenile myoclonic epilepsy and complex partial seizures. *Neurology* **2001**, *56*, 709–715.
- Horinishi, H.; Grillo, M.; Margolis, F. L. Purification and characterization of carnosine synthetase from mouse olfactory bulbs. *J. Neurochem.* **1978**, *31*, 909–919.
- Nagai, K.; Nijima, A.; Yamano, T.; Otani, H.; Okumura, N.; Tsuruoka, N.; Nakai, M.; Kiso, Y. Possible role of L-carnosine in the regulation of blood glucose through controlling autonomic nerves. *Exp. Biol. Med. (Maywood, NJ, U.S.)* **2003**, *228*, 1138–1145.
- Pegova, A.; Abe, H.; Boldyrev, A. Hydrolysis of carnosine and related compounds by mammalian carnosinases. *Comp. Biochem. Physiol., B* **2000**, *127*, 443–446.
- Lenney, J. F.; Peppers, S. C.; Kucera-Orallo, C. M.; George, R. P. Characterization of human tissue carnosinase. *Biochem. J.* **1985**, *228*, 653–660.
- Lenney, J. F.; George, R. P.; Weiss, A. M.; Kucera, C. M.; Chan, P. W.; Rinzler, G. S. Human serum carnosinase: characterization, distinction from cellular carnosinase, and activation by cadmium. *Clin. Chim. Acta* **1982**, *123*, 221–231.
- Jackson, M. C.; Kucera, C. M.; Lenney, J. F. Purification and properties of human serum carnosinase. *Clin. Chim. Acta* **1991**, *196*, 193–205.
- Teufel, M.; Saudek, V.; Ledig, J. P.; Bernhardt, A.; Boularand, S.; Carreau, A.; Cairns, N. J.; Carter, C.; Cowley, D. J.; Duverger, D.; Ganzhorn, A. J.; Guenet, C.; Heintzelmann, B.; Laucher, V.; Sauvage, C.; Smirnova, T. Sequence identification and characterization of human carnosinase and a closely related nonspecific dipeptidase. *J. Biol. Chem.* **2003**, *278*, 6521–6531.
- Lenney, J. F.; Peppers, S. C.; Kucera, C. M.; Sjaastad, O. Homocarnosinosis: lack of serum carnosinase is the defect probably responsible for elevated brain and CSF homocarnosine. *Clin. Chim. Acta* **1983**, *132*, 157–165.
- Kramarenko, G. G.; Markova, E. D.; Ivanova-Smolenskaya, I. A.; Boldyrev, A. A. Peculiarities of carnosine metabolism in a patient with pronounced homocarnosinemia. *Bull. Exp. Biol. Med.* **2001**, *132*, 996–999.
- Wassif, W. S.; Sherwood, R. A.; Amir, A.; Idowu, B.; Summers, B.; Leigh, N.; Peters, T. J. Serum carnosinase activities in central nervous system disorders. *Clin. Chim. Acta* **1994**, *225*, 57–64.
- Butterworth, R. J.; Wassif, W. S.; Sherwood, R. A.; Gerges, A.; Poyser, K. H.; Garthwaite, J.; Peters, T. J.; Bath, P. M. Serum neuron-specific enolase, carnosinase, and their ratio in acute stroke. An enzymatic test for predicting outcome? *Stroke* **1996**, *27*, 2064–2068.
- Janssen, B.; Hohenadel, D.; Brinkkoetter, P.; Peters, V.; Rind, N.; Fischer, C.; Rychlik, I.; Cerna, M.; Romzova, M.; de Heer, E.; Baelde, H.; Bakker, S. J.; Zirie, M.; Rondeau, E.; Mathieson, P.; Saleem, M. A.; Meyer, J.; Koppel, H.; Sauerhoefer, S.; Bartram, C. R.; Nawroth, P.; Hammes, H. P.; Yard, B. A.; Zschocke, J.; van der Woude, F. J. Carnosine as a protective factor in diabetic nephropathy: association with a leucine repeat of the carnosinase gene CNDP1. *Diabetes* **2005**, *54*, 2320–2327.
- The model based on amino peptidase PepV, generated by Fugue, was refined using the same computational procedures described in Computational Methods for the model based on  $\beta$ -alanine synthase.
- Testa, B.; Mayer, J. M. *Hydrolysis in Drug and Prodrug Metabolism—Chemistry, Biochemistry and Enzymology*, Wiley-VHCA: Zurich, Switzerland, 2003; pp 48–65.
- Monod, J.; Changeux, J. P.; Jacob, F. Allosteric proteins and cellular control systems. *J. Mol. Biol.* **1963**, *6*, 306–329.
- Monod, J.; Wyman, J.; Changeux, J. P. On the nature of allosteric transitions: a plausible model. *J. Mol. Biol.* **1965**, *12*, 88–118.
- MacDonald, J.; Storey, K. B. Temperature and phosphate effects on allosteric phenomena of phosphofructokinase from a hibernating ground squirrel (*Spermophilus lateralis*). *FEBS J.* **2005**, *272*, 120–128.
- Song, E. S.; Hersh, L. B. Insulysin: An allosteric enzyme as a target for Alzheimer's disease. *J. Mol. Neurosci.* **2005**, *25*, 201–206.
- Islam, M. N.; Sueda, S.; Kondo, H. Construction of new forms of pyruvate carboxylase to assess the allosteric regulation by acetyl-CoA. *Protein Eng., Des. Sel.* **2005**, *18*, 71–78.
- Willemoes, M.; Molgaard, A.; Johansson, E.; Martinussen, J. Lid L11 of the glutamine amidotransferase domain of CTP synthase mediates allosteric GTP activation of glutaminase activity. *FEBS J.* **2005**, *272*, 856–864.
- Childers, S. R.; Li, X.; Xiao, R.; Eisenach, J. C. Allosteric modulation of adenosine A1 receptor coupling to G-proteins in brain. *J. Neurochem.* **2005**, *93*, 715–723.
- Chen, F.; Larsen, M. B.; Neubauer, H. A.; Sanchez, C.; Plenge, P.; Wiborg, O. Characterization of an allosteric citalopram-binding site at the serotonin transporter. *J. Neurochem.* **2005**, *92*, 21–28.
- Lou, X.; Scheuss, V.; Schneggenburger, R. Allosteric modulation of the presynaptic Ca<sup>2+</sup> sensor for vesicle fusion. *Nature* **2005**, *435*, 497–501.
- Stvolinsky, S. L.; Dobrota, D. Anti-ischemic activity of carnosine. *Biochemistry (Moscow, Russ. Ed.)* **2000**, *65*, 849–855.
- [http://srs.ebi.ac.uk/srsbin/cgi-bin/wget?\\_id=73\\_661RRn6\\_+\[embl.AccNumber: AX139747\]+e](http://srs.ebi.ac.uk/srsbin/cgi-bin/wget?_id=73_661RRn6_+[embl.AccNumber: AX139747]+e).

- (34) Dyrløv Bendtsen, J.; Nielsen, H.; Von Heijne, G.; Brunak, S. Improved prediction of signal peptides: SignalP 3.0. *J. Mol. Biol.* **2004**, *340*, 783–795.
- (35) <http://www.cbs.dtu.dk/services/SignalP/>.
- (36) Shi, J.; Blundell, T. L.; Mizuguchi, K. FUGUE: sequence-structure homology recognition using environment-specific substitution tables and structure-dependent gap penalties. *J. Mol. Biol.* **2001**, *310*, 243–257.
- (37) Jozic, D.; Bourenkow, G.; Bartunik, H.; Scholze, H.; Dive, V.; Henrich, B.; Huber, R.; Bode, W.; Maskos, K. Crystal structure of the dinuclear zinc aminopeptidase PepV from *Lactobacillus delbrueckii* unravels its preference for dipeptides. *Structure* **2002**, *10*, 1097–1106.
- (38) Lundgren, S.; Gojkovic, Z.; Piskur, J.; Dobritzsch, D. Yeast beta-alanine synthase shares a structural scaffold and origin with dizinc-dependent exopeptidases. *J. Biol. Chem.* **2003**, *278*, 51851–51862.
- (39) Pedretti, A.; Villa, L.; Vistoli, G. VEGA: a versatile program to convert, handle and visualize molecular structure on windows-based PCs. *J. Mol. Graphics Modell.* **2002**, *21*, 47–49.
- (40) Laskowski, R. A.; MacArthur, M. W.; Moss, D. S.; Thornton, J. M. PROCHECK: a program to check the stereochemical quality of protein structures, *J. Appl. Crystallogr.* **1993**, *26*, 283–291.
- (41) Bowie, J. U.; Luthy, R.; Eisenberg, D. A method to identify protein sequences that fold into a known three-dimensional structure, *Science* **1991**, *253*, 164–170.
- (42) Bredow, T.; Jug, K. Theory and range of modern semiempirical molecular orbital methods. *Theor. Chem. Acc.* **2005**, *113*, 1–14.
- (43) Rarey, M.; Kramer, B.; Lengauer, T.; Klebe, G. A fast flexible docking method using an incremental construction algorithm. *J. Mol. Biol.* **1996**, *261*, 470–489.
- (44) Kalé, L.; Skeel, R.; Bhandarkar, M.; Brunner, R.; Gursoy, A.; Krawetz, N.; Phillips, J.; Shinozaki, A.; Varadarajan, K.; Schulten, K. NAMD2: Greater scalability for parallel molecular dynamics. *J. Comput. Phys.* **1999**, *151*, 283–312.
- (45) Frishman, D.; Argos, P. Knowledge-based protein secondary structure assignment. *Proteins* **1995**, *23*, 566–579.

JM0602099